Journal of Alzheimer's Disease xx (20xx) x–xx
DOI 10.3233/JAD-231413
IOS Press

Distinct and Convergent Alterations of Entorhinal Cortical Circuits in Two Mouse Models for Alzheimer's Disease and Related Disorders

Ping Zhong, Qing Cao and Zhen Yan*
Department of Physiology and Biophysics, Jacobs School of Medicine and Biomedical Sciences, State University of New York at Buffalo, Buffalo, NY, USA

Accepted 6 February 2024

Abstract.
Background: The impairment of neural circuits controlling cognitive processes has been implicated in the pathophysiology of Alzheimer's disease and related disorders (ADRD). However, it is largely unclear what circuits are specifically changed in ADRD, particularly at the early stage.
Objective: Our goal of this study is to reveal the functional changes in the circuit of entorhinal cortex (EC), an interface between neocortex and hippocampus, in AD.
Methods: Electrophysiological, optogenetic and chemogenetic approaches were used to examine and manipulate entorhinal cortical circuits in amyloid-β familial AD model (5 × FAD) and tauopathy model (P301S Tau).
Results: We found that, compared to wild-type mice, electrical stimulation of EC induced markedly smaller responses in subiculum (hippocampal output) of 5 × FAD mice (6-month-old), suggesting that synaptic communication in the EC to subiculum circuit is specifically blocked in this AD model. In addition, optogenetic stimulation of glutamatergic terminals from prefrontal cortex (PFC) induced smaller responses in EC of 5 × FAD and P301S Tau mice (6-month-old), suggesting that synaptic communication in the PFC to EC pathway is compromised in both ADRD models. Chemogenetic activation of PFC to EC pathway did not affect the bursting activity of EC neurons in 5 × FAD mice, but partially restored the diminished EC neuronal activity in P301S Tau mice.
Conclusions: These data suggest that 5 × FAD mice has a specific impairment of short-range hippocampal gateway (EC to subiculum), which may be caused by amyloid-β deposits; while two ADRD models have a common impairment of long-range cortical to hippocampal circuit (PFC to EC), which may be caused by microtubule/tau-based transport deficits. These circuit deficits provide a pathophysiological basis for unique and common impairments of various cognitive processes in ADRD conditions.

Keywords: Alzheimer's disease, electrophysiology, entorhinal cortex, 5×FAD, neural circuits, optogenetics, P301S Tau, prefrontal cortex, subiculum

INTRODUCTION

The most prominent brain regions impaired at early stages of Alzheimer's disease (AD) include prefrontal cortex (PFC), and hippocampal formation that comprises the hippocampus proper (CA1, CA2, CA3),

*Correspondence to: Zhen Yan, Department of Physiology and Biophysics, Jacobs School of Medicine and Biomedical Sciences, State University of New York at Buffalo, Buffalo, NY 14203, USA. E-mail: zhenyan@buffalo.edu.

ISSN 1387-2877/$35.00

dentate gyrus, and subiculum [1–9]. PFC is responsible for executive function and working memory [10–12], while hippocampus is essential for memory consolidation and storage [13]. There are strong connections between PFC and hippocampal formation, which is vital for sustaining complex memory processing [14–17]. Given the loss of coordination between executive function and stored memory in AD patients [18, 19], PFC-hippocampal connections may be compromised in AD.

While hippocampal neurons send direct outputs to PFC [15, 20, 21], projections from PFC to hippocampus usually go through the interface, entorhinal cortex (EC) [22–24]. EC acts as a gateway in memory processing, transferring information that is encoded and organized in PFC to hippocampus for consolidation, and retrieving contextual information stored in hippocampus to PFC for goal-directed behaviors [20, 25–28]. EC sends extensive projections to CA1 and subiculum [29–32]. As the hippocampal output, subiculum innervates various downstream regions, controlling interregional communication in the hippocampal-parahippocampal circuit [31, 33–36].

Dysfunction of EC has been implicated in AD [37–40]. However, it remains largely unknown about how synaptic signals along the PFC-EC-subiculum axis are disrupted in AD conditions associated with amyloid plaques or neurofibrillary tangles. To address this question, we used electrophysiological and optogenetic approaches to examine the local and long-range functional circuits in two different AD mouse models, the familial AD mice carrying 5 mutations on APP and PS1 (5 × FAD) and the transgenic mice carrying human P301S mutation of microtubule-associated protein tau (P301S Tau). The precise mapping of circuit changes at early symptomatic stage of AD will help to pinpoint intervene loci for symptom alleviation.

MATERIALS AND METHODS

Animals, viruses, and surgery

Animal use was approved by the IACUC of State University of New York at Buffalo. 5 × FAD mice (Jackson Laboratory, 034848), Tau P301S transgenic mice [41] (Jackson Laboratory, 008169) and their wild-type controls were genotyped and used as we previously described [2, 42–44].

AAV9.CAG.hChR2(H134R)-mCherry.WPRE.SV40 (ChR2), AAV9-hSyn-HI-eGFP-Cre (Cre) and AAVrg-hSyn-DIO-hM3D(Gq)-mCherry (RetroGq) were purchased from Addgene. Virus injection was conducted as previously described [45–48]. Briefly, mice (∼6 months old) were anesthetized with ketamine (95 mg/kg) and xylazine (5 mg/kg). Then ChR2 virus (1 μl) or Cre virus (1 μl) was stereotaxically injected into the prelimbic cortex bilaterally (AP: 2.0 mm, ML:±0.3 mm, DV: 2 mm), and RetoGq virus (1 μl) was injected into the entorhinal cortex (EC) (AP: –4.7 mm, ML:±3.0 mm, DV: 3.2 mm) with a Hamilton syringe (31 gauge). Injection speed was controlled with a microinjection pump (KD Scientific) (100 nl/min). Mice were used 6 weeks after the viral injection. For chemogenetic studies, electrophysiological recordings started 1 h after intraperitoneal injection of CNO (5 mg/kg) or saline in virus-infected mice.

Electrophysiological and optogenetic recordings

Mice were anesthetized with isoflurane and rapidly decapitated. Brains were quickly removed and submerged into the ice-cold sucrose solution (in mM: 234 sucrose, 4 $MgSO_4$, 2.5 KCl, 1 NaH_2PO_4, 0.1 $CaCl_2$, 15 HEPES, 11 glucose, pH 7.35). Sagittal slices (300 μm) containing EC and subiculum regions were cut on a vibratome (Leica VT1000 s), then transferred into artificial cerebrospinal fluid (ACSF) (in mM: 130 NaCl, 26 $NaHCO_3$, 3 KCl, 5 $MgCl_2$, 1.25 NaH_2PO_4, 1 $CaCl_2$, 10 Glucose, pH 7.4, 300 mOsm, 95% O_2 + 5% CO_2), and kept at 32°C for 1 h and then at the room temperature (22–24°C) for 1–4 h.

For recordings, the slice was positioned in a perfusion chamber attached to the fixed stage of an upright microscope (Olympus) and submerged in continuously flowing oxygenated ACSF. Whole-cell patch-clamp experiments were performed with a Multi-clamp 700A amplifier and Digidata 1322A data acquisition system (Molecular Devices). Neurons were visualized with the infrared differential interference contrast video microscopy. Data were acquired using the software Clampex 9.2 (Molecular Device). Recording electrodes were pulled from borosilicate glass capillaries (1.5/0.86 mm OD/ID) with a micropipette puller (Sutter Instrument, model P-97). The resistance of patch electrode was 3–4 MΩ.

Optogenetic stimulation of ChR2-expressing neurons or terminals in brain slices was carried out via a microscope objective (Olympus LUMPlan FI/IR, 40 × 0.80 w) using a UHP-Microscope-LED-460

system (Prizmatix) that provides >1 W collimated blue light (460 nm peak, 27 nm spectrum half width, 85% peak power at 450 nm). The blue light was triggered with TTL pulses programmed by the pClamp (Molecular Devices) data acquisition software. Single light pulses (5 ms) were delivered during electrophysiological recordings.

Whole-cell voltage clamp was used to measure spontaneous excitatory postsynaptic current (sEPSC), EPSC evoked by electrical stimulation of neighboring neurons (eEPSC), and EPSC evoked by optogenetic stimulation of ChR2-expressing neurons or terminals (opto-EPSC). Cells were held at –70 mV, and $GABA_AR$ blocker bicuculline (10 μM) was added to ACSF during EPSC recordings. The internal solution contained (in mM): 130 Cs-methanesulfonate, 10 CsCl, 4 NaCl, 1 $MgCl_2$, 5 EGTA, 10 HEPES, 4 ATP, 0.5 GTP, and 10 phosphocreatine. Whole-cell current clamp was used to record synaptic-driven spontaneous action potential (sAP) firing and the internal solution contained (in mM): 20 KCl, 100 K-gluconate, 10 HEPES, 4 ATP, 0.5 GTP, and 10 phosphocreatine. In sAP recordings, a modified ACSF with lower (0.5 mM) $MgCl_2$ and higher (3.5 mM) KCl was used to increase neuronal activity in slices, and a small (<50 pA) adjusting current (positive DC) was injected to elevate the membrane potential (inter-spike potential: –60 mV) [49, 50].

Immunofluorescent staining

After viral expression, mice were anesthetized and transcardially perfused as we previously described [2, 42]. In brief, brain tissue was post-fixed in 4% paraformaldehyde and dehydrated with 30% sucrose for 2 days. Coronal sections (50 μm) were cut with a vibrating microtome (Leica VT1000S) and stored in cryoprotectant solution at –20°C until ready to use. For illustrating the viral expression of ChR2(H134R)-mCherry in PFC, slices were blocked with PBS containing 5% goat serum (1 h, room temperature), followed by PBS washing and direct imaging with a Leica DMi8 fluorescence inverted microscope with Spiral function at 10×magnification. For labeling PFC neurons, slices were incubated with anti-NeuN (1 : 500; Millipore, MAB377). After washing, slices were incubated with a fluorescent secondary antibody (A-11055, 1 : 1000, ThermoFisher Scientific) at room temp for 1 h. Images were acquired by using a Leica TCS SP8 confocal microscope.

Data analysis

Data analyses were performed with the Clampfit software (Molecular Devices), Mini Analysis Program (Synaptosoft), and KaleidaGraph software. Statistical analysis was performed with Prism (GraphPad). Two-way ANOVA or 2-tailed unpaired Student's *t*-test were used to determine the significance of differences between groups. All data are expressed as the mean ± SEM.

RESULTS

Impairment of entorhinal cortex → Subiculum circuit in AD

Since EC → subiculum pathway comprises the major hippocampal input → output gateway, we first examined the potential alteration of this circuit in AD models by stimulating EC and recording evoked EPSC in subiculum (Fig. 1A). As shown in Fig. 1B and 1C, the synaptic signal in EC → subiculum circuit was largely abolished in 6-month-old 5 × FAD mice (WT: 47.8 ± 6.2 pA, $n = 13$ cells/3 mice, FAD: 10.3 ± 3.1 pA, $n = 20$ cells/5 mice, $t_{31} = 5.9$, $p < 0.001$, *t*-test), but was not significantly changed in 6-month-old P301S Tau mice (Fig. 1D, E; WT: 58.3 ± 6.1 pA, $n = 12$ cells/3 mice, Tau: 42.6 ± 5.7 pA, $n = 13$ cells/4 mice, $t_{23} = 1.8$, $p = 0.08$, *t*-test). Young 5 × FAD mice (3-month-old) had normal EC → subiculum synaptic currents (Fig. 1F, 1 G; WT: 80.7 ± 5.2 pA, $n = 11$ cells/3 mice, FAD: 70.5 ± 4.4 pA, $n = 11$ cells/3 mice, $t_{20} = 1.5$, $p = 0.16$, *t*-test). It suggests that amyloid-β (Aβ) accumulation in 6-month-old 5 × FAD mice blocks synaptic communication from EC to subiculum.

We further examined spontaneous synaptic currents induced by randomly activated synapses that have action potential-independent release of single synaptic vesicles in subiculum (Fig. 2A). As shown in Fig. 2B and 2C, the amplitude and frequency of spontaneous excitatory postsynaptic currents (sEPSC) were modestly but significantly decreased in the subiculum of 6-month-old 5 × FAD mice (Amplitude, WT:13.2 ± 0.4 pA, $n = 10$ cells/3 mice, FAD: 11.6 ± 0.5 pA, $n = 11$ cells/3 mice, $t_{19} = 2.5$, $p = 0.023$, Frequency, WT: 3.75 ± 0.47 Hz, $n = 10$ cells/3 mice, FAD: 2.06 ± 0.46 Hz, $n = 11$ cells/3 mice, $t_{19} = 2.6$, $p = 0.018$, *t*-test). Recordings in the subiculum of P301S Tau mice (6-month-old) did not find significant changes in sEPSC (Fig. 2D, E; Amplitude, WT: 13.4 ± 0.4 pA, $n = 10$

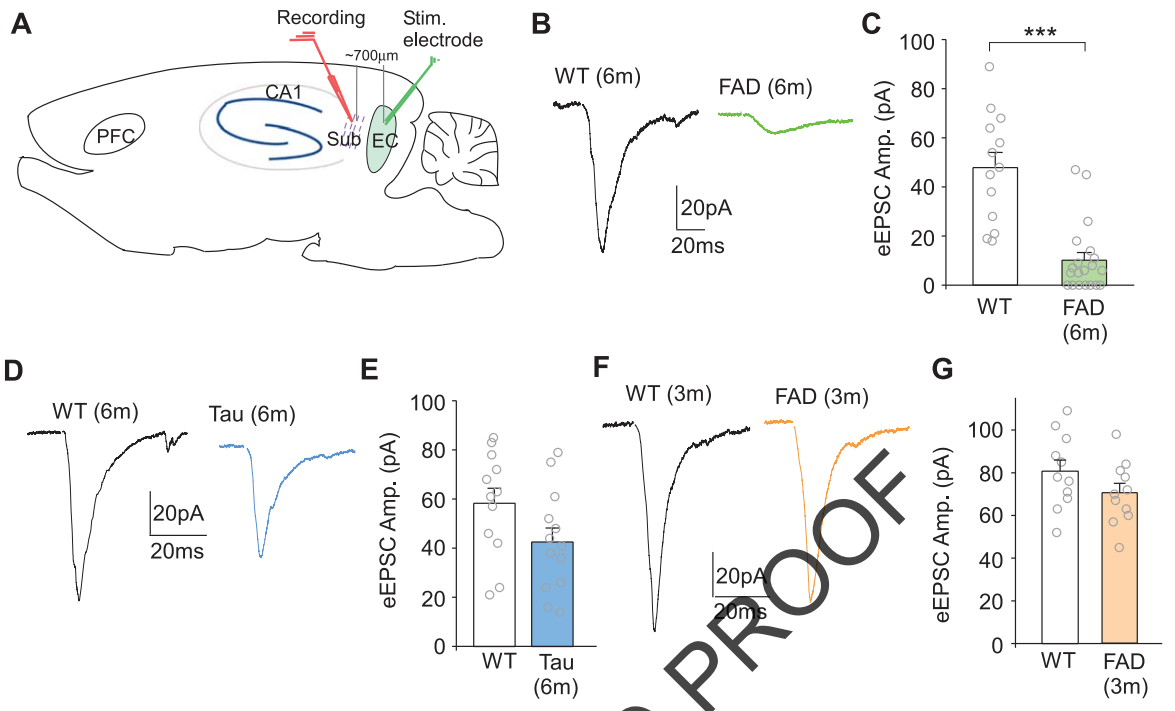

Fig. 1. Specific blockade of synaptic transmission from entorhinal cortex (EC) to subiculum in 5 × FAD mice. A) Diagram showing the location of recording and stimulating electrodes. B) Representative traces of EPSC in subiculum evoked by electrical stimulation of EC in a WT and a 5 × FAD mouse (6-month-old). C) Bar graphs of eEPSC amplitudes in EC of WT and 5 × FAD mice (6-month-old). ***$p < 0.001$, *t*-test. D, E) Representative eEPSC traces (D) and bar graphs of eEPSC amplitudes (E) in EC of WT and P301S Tau mice (6-month-old). F, G) Representative eEPSC traces (F) and bar graphs of eEPSC amplitudes (G) in EC of young WT and 5 × FAD mice (3-month-old).

cells/3 mice, Tau:12.2 ± 0.6 pA, $n = 10$ cells/3 mice, $t_{18} = 1.7$, $p = 0.11$, Frequency, WT:3.44 ± 0.28 Hz, Tau: 3.01 ± 0.27 Hz, $t_{18} = 1.1$, $p = 0.27$, *t*-test). In young 5 × FAD mice (3-month-old), sEPSC in subiculum was intact (Fig. 2F: Amplitude, WT: 13.7 ± 0.5 pA, $n = 10$ cells/2 mice, FAD:13.2 ± 0.3 pA, $n = 10$ cells/3 mice, $t_{18} = 0.9$, $p = 0.37$, Frequency, WT:4.08 ± 0.52 Hz, FAD: 3.37 ± 0.34 Hz, $t_{18} = 1.2$, $p = 0.26$, *t*-test).

Synaptic activity drives the firing of action potentials. Next, we examined synaptic-driven spontaneous action potential (sAP) in subiculum of AD models. As shown in Fig. 2G and 2H, the frequencies of sAP were substantially decreased (~50%) in subiculum of 6-month-old 5 × FAD mice (WT: 7.82 ± 0.67 Hz, $n = 12$ cells/3 mice, FAD: 4.13 ± 0.75 Hz, $n = 12$ cells/3 mice, $t_{22} = 4.2$, $p = 0.0003$, *t*-test). A less pronounced, but significant, reduction (~30%) of sAP frequencies was also found in 6-month-old Tau mice (Fig. 2I, J; WT: 5.79 ± 0.71 Hz, $n = 11$ cells/3 mice, Tau: 3.88 ± 0.52 Hz, $n = 12$ cells/3 mice, $t_{21} = 2.7$, $p = 0.02$, *t*-test). It suggests that neuronal excitability of subiculum is reduced in AD models, most strikingly in 5 × FAD mice.

Alteration of prefrontal cortex → Entorhinal cortex circuit in AD.

The hippocampal formation receives inputs from PFC via EC. Next, we examined the potential alteration of PFC → EC circuit in AD conditions. We first examined synaptic transmission within EC by stimulating local neurons. As shown in Fig. 3A, the amplitudes of EPSC evoked by a series of stimuli in EC pyramidal neurons of 6-month-old 5 × FAD mice were largely unchanged, compared to age-matched WT mice ($n = 9$ cells/3 mice/ group, $F_{1,16} = 2.3$, $p = 0.15$, two-way rmANOVA). The amplitude and frequency of sEPSC in EC were also similar between WT versus FAD mice (WT: 14.3 ± 0.5 pA, 5.73 ± 0.48 Hz; FAD: 13.1 ± 0.4 pA, 4.76 ± 0.52 Hz, $p = 0.1$ (Amp.), $p = 0.2$ (Freq.), *t*-test). We further examined synaptic signals in EC of 6-month-old P301S Tau mice. As shown in Fig. 3C and 3D, the input-output curves of evoked EPSC were similar in

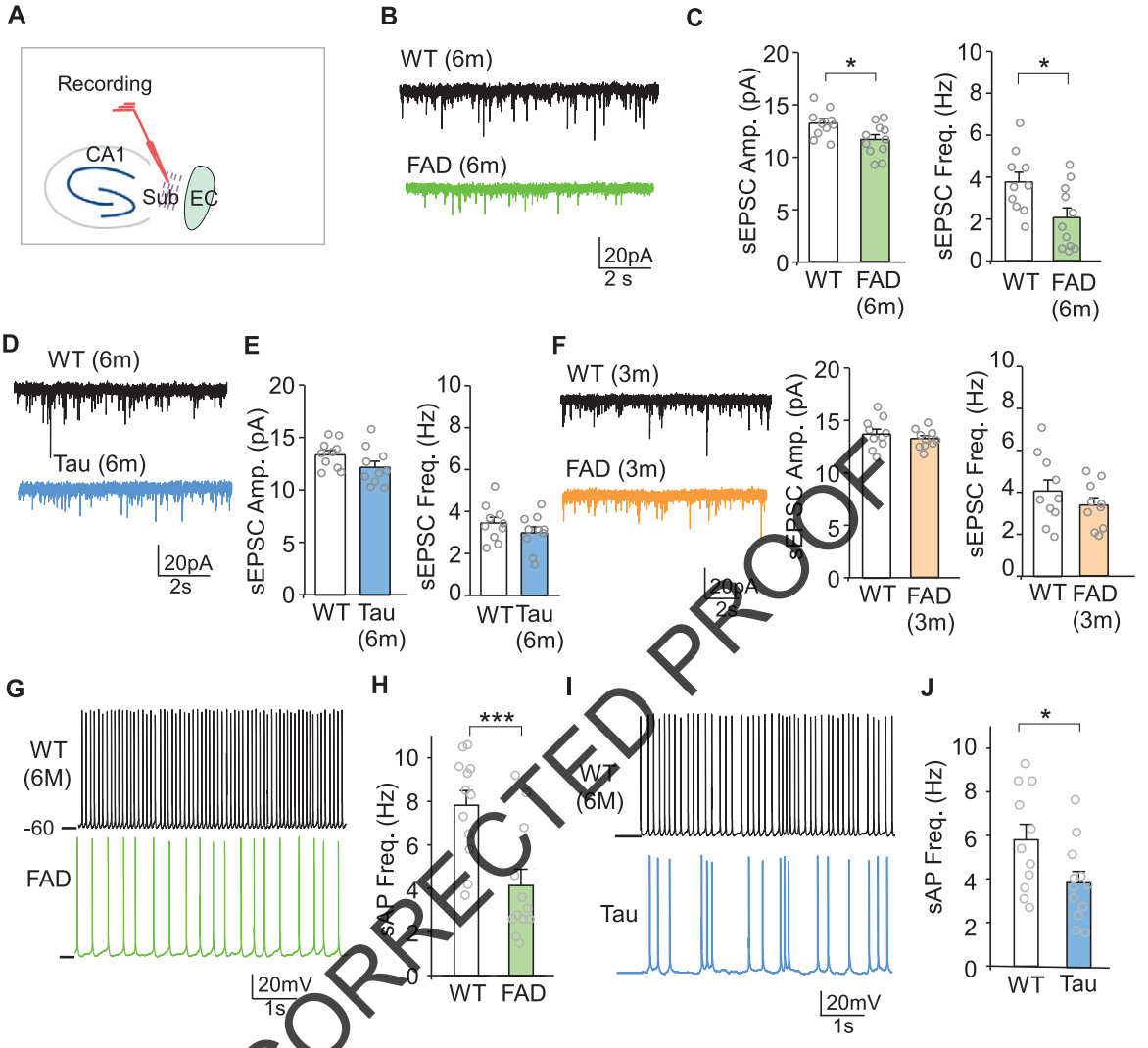

Fig. 2. Alteration of synaptic and neuronal activity in subiculum of AD models. A) Diagram showing the experiment setting. B, C) Representative sEPSC traces (B) and bar graphs of sEPSC amplitudes and frequencies (C) in subiculum of 6-month-old WT versus 5 × FAD mice. $^{*}p<0.05$, *t*-test. D, E) Representative sEPSC traces (D) and bar graphs of sEPSC amplitudes and frequencies (E) in subiculum of 6-month-old WT versus P301S Tau mice. F) Representative sEPSC traces and bar graphs of sEPSC amplitudes and frequencies in subiculum of 3-month-old WT versus 5 × FAD mice. G, H) Representative sAP recording traces (G) and bar graphs of sAP frequencies (H) in subiculum of 6-month-old WT versus 5 × FAD mice. $^{***}p<0.001$, *t*-test. I, J) Representative sAP traces (I) and bar graphs of sAP frequencies (J) in subiculum of 6-month-old WT versus P301S Tau mice. $^{*}p<0.05$, *t*-test.

EC of WT versus Tau mice ($n=8$ cells/3 mice/group, $F_{1,14}$ =2.1, $p=0.18$, two-way rmANOVA). The amplitude and frequency of sEPSC in EC of Tau mice were also unchanged (WT: 14.6 ± 0.7 pA, 6.49 ± 0.65 Hz, Tau: 13.8 ± 0.7 pA, 5.65 ± 0.61 Hz, $p=0.4$, *t*-test).

Next, we conducted optogenetic experiments to examine the PFC → EC pathway. ChR2(H134 R)-mCherry AAV was injected into PFC, and electrophysiological recordings were performed on EC neurons with light stimulation of synaptic inputs from PFC (Fig. 4A). Confocal images (Fig. 4A, B) showed the expression of ChR2 in PFC neurons at the virus injection site and the expression of ChR2 at synaptic terminals in EC originating from PFC projections. As shown in Fig. 4C, the amplitudes of EPSC evoked by optogenetic stimulation of PFC projections were significantly decreased in 5 × FAD mice (WT: 55.5 ± 5.2 pA, $n=11$ cells/3 mice, FAD: 38.5 ± 4.1 pA, $n=12$ cells/4 mice, $t_{21}=2.6$, $p=0.017$, *t*-test). A similar reduction of opto-EPSC was also observed in EC of Tau mice (Fig. 4D; WT: 51.7 ± 5.8 pA, $n=13$

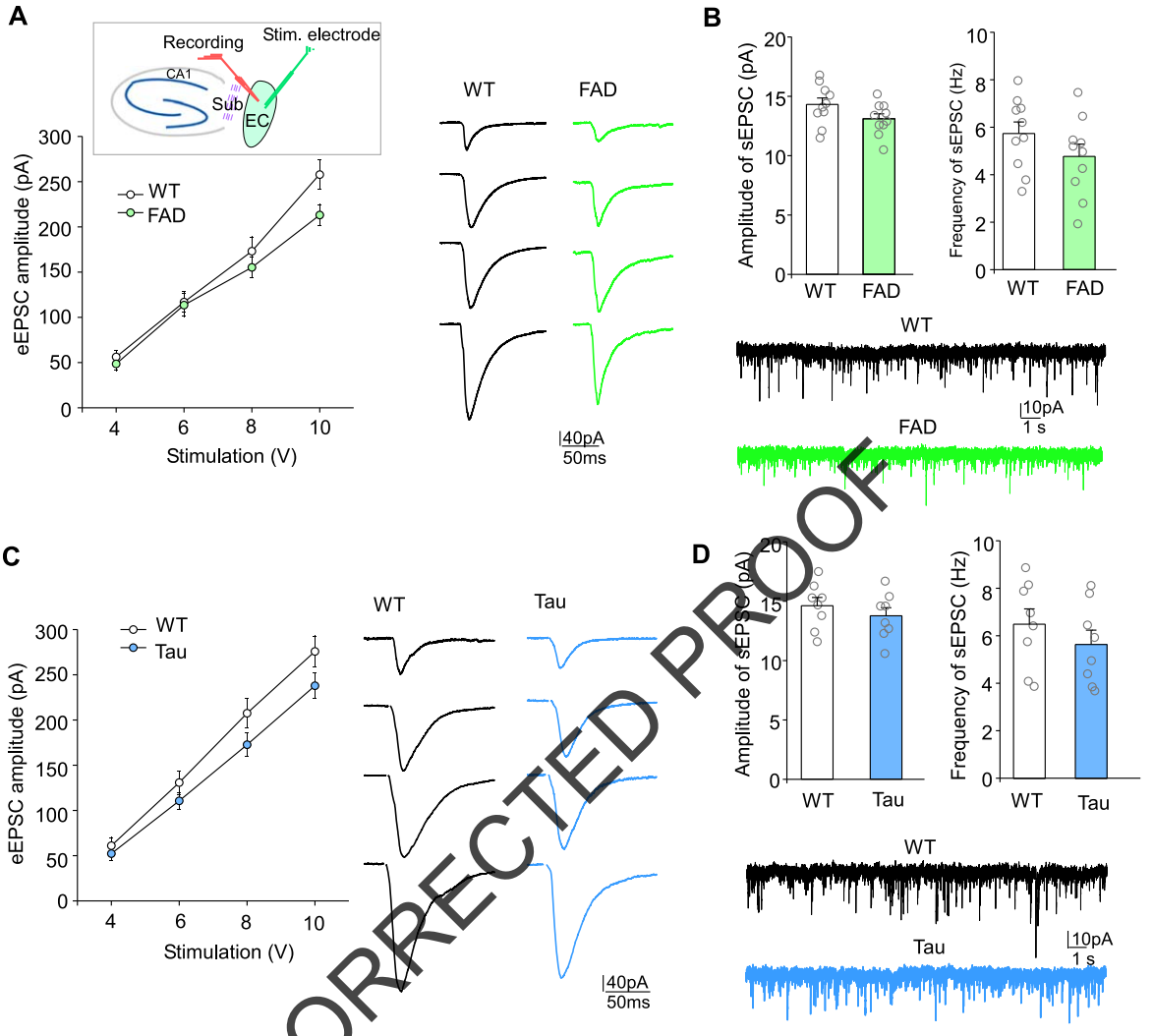

Fig. 3. Unchanged EC local circuit in AD models. A) Plot showing the input-output curve of EPSC in EC neurons evoked by stimulating neighboring cells in WT versus 5 × FAD mice (6-month-old). Inset, upper: diagram showing experiment setting; right: representative eEPSC traces. B) Bar graph showing the amplitude and frequency of sEPSC in EC neurons from WT versus 5 × FAD mice (6-month-old). Inset, representative sEPSC traces. C) Input-output curve of EPSC in EC neurons evoked by stimulating neighboring cells in WT versus P301S Tau mice (6-month-old). Inset, representative eEPSC traces. D) Bar graph showing the amplitude and frequency of sEPSC in EC neurons from WT versus P301S Tau mice (6-month-old). Inset, representative sEPSC traces.

cells/3 mice, Tau: 32.1 ± 4.6 pA, $n = 14$ cells/4 mice, $t_{25} = 2.7$, $p = 0.013$, t-test). These data suggest that the long-range PFC to EC pathway is impaired in both AD models.

Chemogenetic manipulation of prefrontal cortex → Entorhinal cortex circuit in AD.

Given the compromised PFC to EC projection in AD models, we next used chemogenetic activation of PFC → EC pathway to examine the possibility of restoring EC neuronal activity in AD. The GFP-tagged Cre virus (AAV9-hSyn-HI-eGFP-Cre) was injected bilaterally to PFC, and the mCherry-tagged retrograde double floxed DREADD (AAVrg-hSyn-DIO-hM3D(Gq)-mCherry) virus was injected into the EC (Fig. 5A). Selective manipulation of the PFC to EC pathway was achieved by the systemic administration of CNO (3 mg/kg, i.p.) at 6 weeks post-injection. The validity of using such a method to manipulate the activity of specific circuits has been demonstrated by our previous imaging, elec-

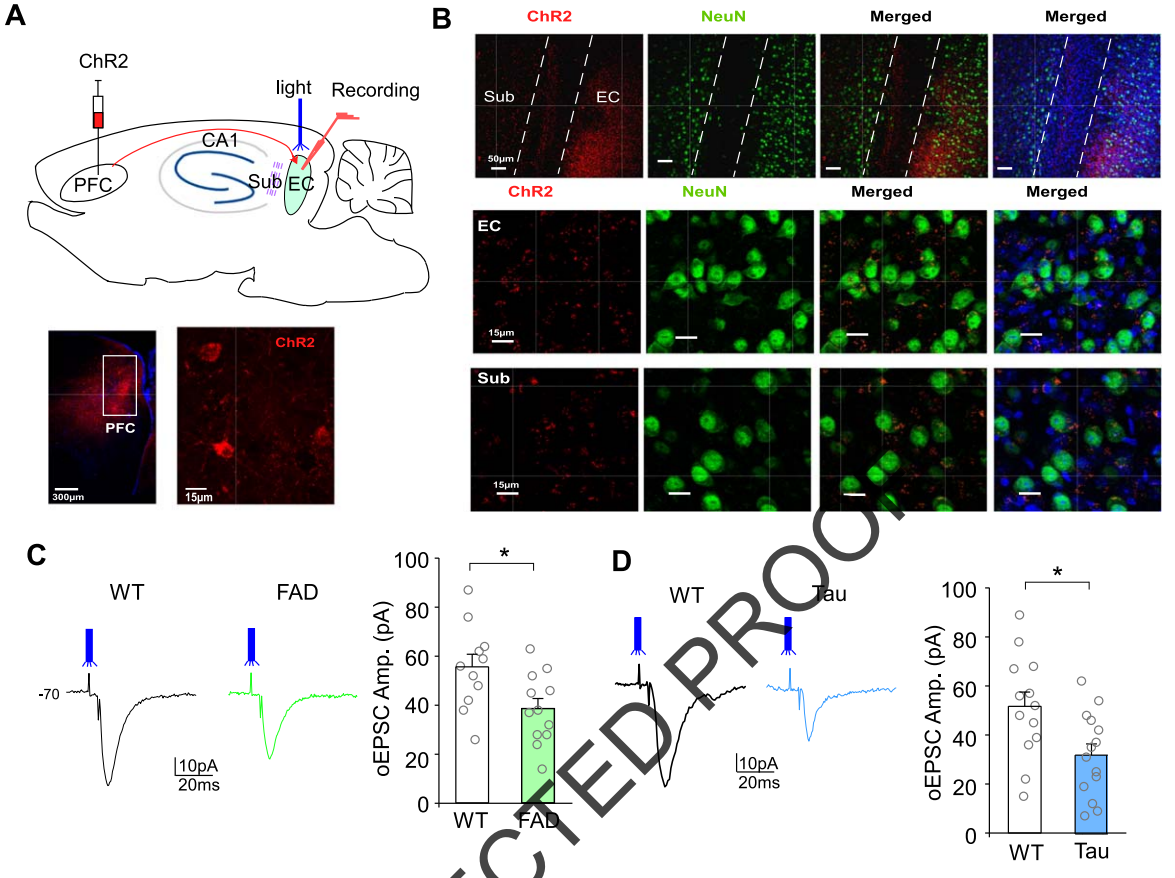

Fig. 4. Diminished synaptic transmission from prefrontal cortex (PFC) to EC in AD models. A) Upper, diagram showing experiment setting. Bottom, confocal images showing the viral expression of ChR2(H134R)-mCherry in PFC. B) Confocal images showing ChR2 (red)-expressing terminals around neurons (NeuN+, green) in EC and subiculum areas. C) Representative opto-EPSC traces evoked by blue light stimulation of ChR2 + terminals and bar graphs of opto-EPSC amplitudes in EC of WT versus 5 × FAD mice (6-month-old). $^{*}p < 0.05$, *t*-test. D) Representative opto-EPSC traces and bar graphs of opto-EPSC amplitudes in EC of WT versus P301S Tau mice (6-month-old). $^{*}p < 0.05$, *t*-test.

trophysiological and biochemical experiments [48, 51–55].

The sAP in EC pyramidal neurons of 5 × FAD mice showed strong bursting activity, which was distinct from the mostly regular pattern of sAP in EC of WT mice, and CNO administration did not alter the bursting firing pattern of 5 × FAD or WT mice (Fig. 5B). The average frequency of sAP (within two minutes of recordings) was significantly lower in EC of 5 × FAD than WT mice, and CNO was ineffective in significantly changing sAP in 5 × FAD mice (Fig. 5C; WT: 1.71 ± 0.17 Hz, $n = 15$ cells/3 mice, FAD: 1.11 ± 0.09 Hz, $n = 16$ cells/4 mice, WT+CNO, 1.77 ± 0.21 Hz, $n = 15$ cells/3 mice, FAD+CNO, 1.25 ± 0.11 Hz, $n = 15$ cells/4 mice, $F_{1,57}$ =13.5, $p = 0.0005$, two-way ANOVA). Further examinations of sAP frequencies during bursting and bursting intervals also found no effect with CNO treatment in 5 × FAD mice (Fig. 5D; bursting freq., FAD+Sal: 10.83 ± 0.36 Hz, FAD+CNO:10.11 ± 0.23 Hz, $p = 0.11$; bursting interval, FAD+Sal: 15.0 ± 0.6 Sec, FAD+CNO: 13.3 ± 0.6 Sec, $p = 0.07$).

We next compared sAP in EC of WT versus Tau mice. No strong bursting activity was observed in EC pyramidal neurons of Tau mice. Compared to WT mice, sAP in EC of Tau mice had substantially lower frequencies, which was significantly elevated by CNO administration (Fig. 5E, F; WT: 1.83 ± 0.21 Hz, $n = 16$ cells/3 mice; Tau: 0.86 ± 0.13 Hz, $n = 18$ cells/4 mice, WT+CNO, 1.93 ± 0.20 Hz, $n = 17$ cells/4 mice, FAD+CNO, 1.51 ± 0.16 Hz, $n = 17$ cells/4 mice, $F_{1,64}$ =15.9, $p = 0.0002$, two-way ANOVA). These data suggest that chemogenetic activation of PFC to EC pathway is capable of partially restoring EC neuronal activity in Tau mice.

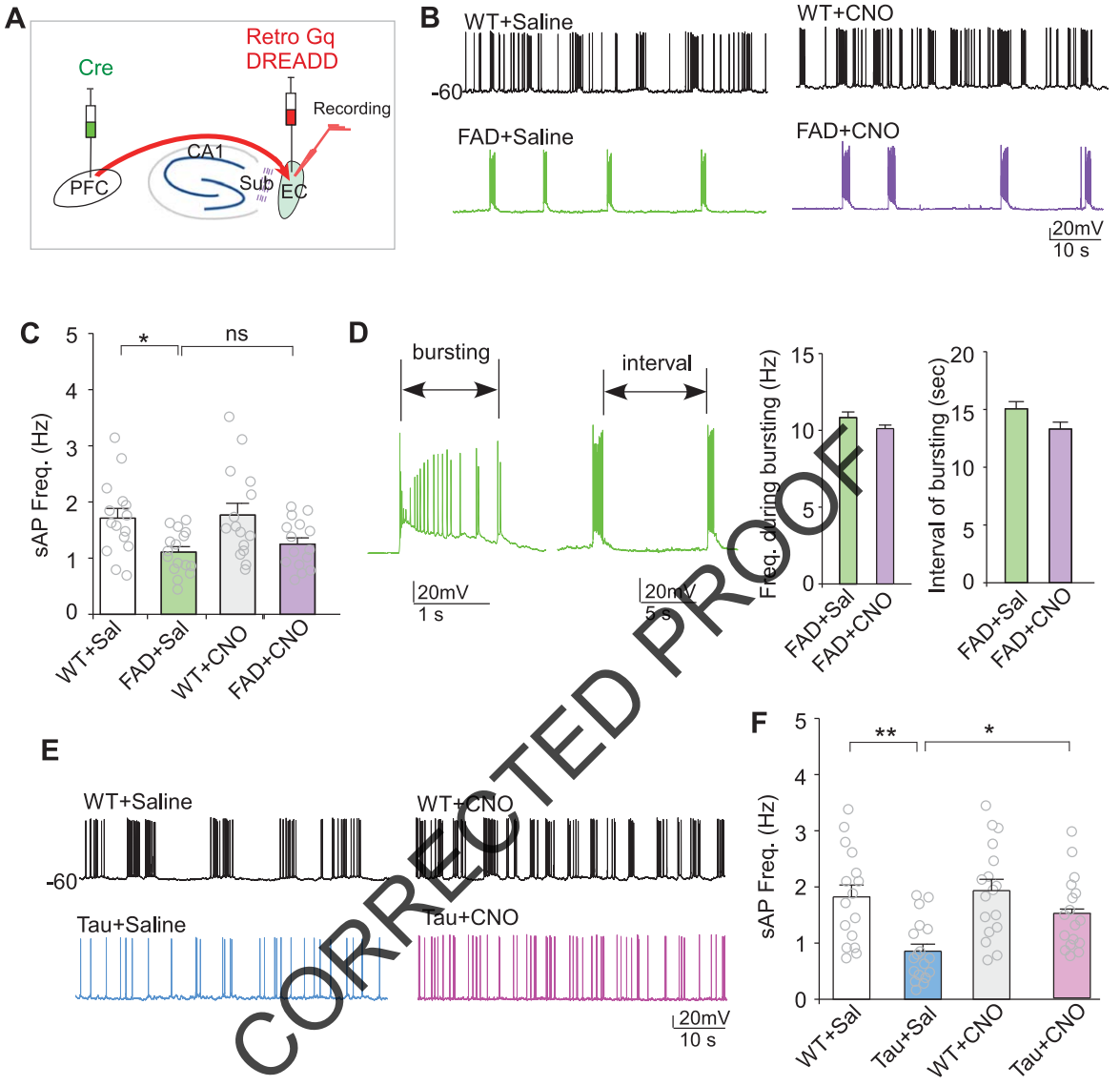

Fig. 5. Partial restoration of EC neuronal activity by chemogenetic stimulation of PFC to EC pathway in P301S Tau mice. A) Diagram showing experiment setting. The GFP-tagged Cre virus (AAV9-hSyn-HI-eGFP-Cre) was injected bilaterally to PFC, and the mCherry-tagged retrograde double floxed DREADD (AAVrg-hSyn-DIO-hM3D(Gq)-mCherry) virus was injected into the EC. After 6 weeks of viral expression, recordings were conducted on EC neurons within hours after saline versus CNO administration. B) Representative sAP recording traces in EC neurons from WT versus 5 × FAD mice (6-month-old) treated with saline or CNO. Note the strong bursting activity in EC of 5 × FAD mice. C) Bar graph showing sAP frequencies in saline- or CNO-treated WT versus 5 × FAD mice. $^{*}p < 0.05$, two-way ANOVA. D) Bar graph showing sAP frequencies during bursting and intervals of bursting in saline- or CNO-treated 5 × FAD mice. Inset, Representative sAP traces. E) Representative sAP recording traces in EC neurons from WT versus P301S Tau mice (6-month-old) treated with saline or CNO. F) Bar graph showing sAP frequencies in saline- or CNO-treated WT versus P301S Tau mice. $^{*}p < 0.05$, $^{**}p < 0.01$, two-way ANOVA.

DISCUSSION

The interactions between PFC and hippocampus play a key role in episodic memory recollection, the process of retrieving contextual information pertaining to a past event or experience [14, 16]. The interruption of communication between PFC and hippocampus affects many forms of learning and memory [17]. As the main interface between hippocampus and neocortex, EC is an important hub to relay information [23] and regulate memory formation and consolidation [22]. By using electrophysiological and optogenetic approaches, we have revealed the functional changes in PFC-EC-

subiculum circuit in two models for ADRD. We found that synaptic communication in the EC → subiculum circuit was specifically blocked in 5 × FAD mice, while synaptic communication in the PFC → EC pathway was compromised in both 5 × FAD and P301S Tau mice. Chemogenetic activation of PFC → EC pathway partially restored the diminished EC neuronal activity in P301S Tau mice.

One of the main targets of EC in the hippocampal system is subiculum [56–58]. Subiculum plays a particularly important role as a key source of hippocampal projections [36]. The brain region with the earliest and highest level of Aβ plaque in 5 × FAD mice is subiculum [59]. The specific loss of EC → subiculum synaptic communication in 6-month-old 5 × FAD mice, but not 6-month-old P301S Tau mice or 3-month-old 5 × FAD mice (Fig. 1), suggests that Aβ accumulation in subiculum has blocked the hippocampal input to hippocampal output gateway. The specific reduction of local synaptic signals within subiculum of 6-month-old 5 × FAD mice (Fig. 2A–F) could also result from Aβ deposits. We further measured spontaneous action potentials (sAP) in subiculum neurons, which are driven by integrated synaptic inputs from local, short-range and long-range projections. The reduction of sAP frequency in subiculum neurons from both 6-month-old 5 × FAD and P301S Tau mice (Fig. 2G–J) suggests that Aβ deposits and tau pathology [41, 59] have impaired inputs to subiculum, leading to the diminished subiculum activity and hippocampal output.

PFC exerts top-down control over hippocampus via EC [22, 60]. Our optogenetic experiments have revealed the significant reduction of PFC → EC synaptic communication in both ADRD models (Fig. 4). Microtubule/tau-based transport deficits are likely the main contributing factors for this impairment of long-range cortical to hippocampal circuit. We further tested whether chemogenetic activation of PFC → EC pathway could restore EC neuronal excitability in AD. One interesting finding is the alteration of sAP firing patten in EC neurons of 6-month-old 5 × FAD mice: while WT mice exhibited regular or mild bursting firing, 5 × FAD mice exhibited the strong rhythmic bursting. CNO application to stimulate PFC → EC pathway did not reverse sAP changes in 5 × FAD mice, but elevated the reduced sAP frequency in P301S Tau mice (Fig. 5). It suggests that strengthening the PFC inputs could partially restore the EC gateway to hippocampal formation in AD associated with tau aberrations.

Taken together, this study has revealed distinct and convergent alterations of entorhinal cortical circuits in two ADRD models. The specific impairment of short-range hippocampal gateway (EC to subiculum) in 6-month-old 5 × FAD mice suggests that hippocampus-mediated memory storage and consolidation are compromised by Aβ deposits. The common impairment of long-range cortical to hippocampal circuit (PFC to EC) in two ADRD models suggests that PFC-mediated memory encoding and retrieval, as well as information organization and processing, are disrupted, probably due to deficiencies in the transport of important cargos along the pathway. These circuit changes provide a pathophysiological basis for various cognitive alterations in ADRD conditions.

AUTHOR CONTRIBUTIONS

Ping Zhong (Data curation; Formal analysis; Writing – original draft); Qing Cao (Data curation; Formal analysis); Zhen Yan, Ph.D. (Conceptualization; Supervision; Writing – review & editing).

ACKNOWLEDGMENTS

We thank Xiaoqing Chen for her excellent technical support.

FUNDING

This work was supported by grants from the National Institutes of Health (AG079797, AG064656) to Z.Y.

CONFLICT OF INTEREST

The authors have no conflict of interest.

DATA AVAILABILITY

Data will be made available on request.

REFERENCES

[1] Zhong P, Cao Q, Yan Z (2022) Selective impairment of circuits between prefrontal cortex glutamatergic neurons and basal forebrain cholinergic neurons in a tauopathy mouse model. *Cereb Cortex* **32**, 5569-5579.

[2] Cao Q, Wang W, Williams JB, Yang F, Wang ZJ, Yan Z (2020) Targeting histone K4 trimethylation for treatment of cognitive and synaptic deficits in mouse models of Alzheimer's disease. *Sci Adv* **6**, eabc8096.

[3] Sun Q, Zhang J, Li A, Yao M, Liu G, Chen S, Luo Y, Wang Z, Gong H, Li X, Luo Q (2022) Acetylcholine deficiency disrupts extratelencephalic projection neurons in the prefrontal cortex in a mouse model of Alzheimer's disease. *Nat Commun* **13**, 998.

[4] Mori T, Shimada H, Shinotoh H, Hirano S, Eguchi Y, Yamada M, Fukuhara R, Tanimukai S, Zhang MR, Kuwabara S, Ueno S, Suhara T (2014) Apathy correlates with prefrontal amyloid beta deposition in Alzheimer's disease. *J Neurol Neurosurg Psychiatry* **85**, 449-455.

[5] Zhuo JM, Prakasam A, Murray ME, Zhang HY, Baxter MG, Sambamurti K, Nicolle MM (2008) An increase in Aβ42 in the prefrontal cortex is associated with a reversal-learning impairment in Alzheimer's disease model Tg2576 APPsw mice. *Curr Alzheimer Res* **5**, 385-391.

[6] Mu Y, Gage FH (2011) Adult hippocampal neurogenesis and its role in Alzheimer's disease. *Mol Neurodegener* **6**, 85.

[7] Vyas Y, Montgomery JM, Cheyne JE (2020) Hippocampal deficits in amyloid-beta-related rodent models of Alzheimer's disease. *Front Neurosci* **14**, 266.

[8] Xu P, Chen A, Li Y, Xing X, Lu H (2019) Medial prefrontal cortex in neurological diseases. *Physiol Genomics* **51**, 432-442.

[9] Small SA, Schobel SA, Buxton RB, Witter MP, Barnes CA (2011) A pathophysiological framework of hippocampal dysfunction in ageing and disease. *Nat Rev Neurosci* **12**, 585-601.

[10] Yan Z, Rein B (2022) Mechanisms of synaptic transmission dysregulation in the prefrontal cortex: Pathophysiological implications. *Mol Psychiatry* **27**, 445-465.

[11] Kesner RP, Churchwell JC (2011) An analysis of rat prefrontal cortex in mediating executive function. *Neurobiol Learn Mem* **96**, 417-431.

[12] Euston DR, Gruber AJ, McNaughton BL (2012) The role of medial prefrontal cortex in memory and decision making. *Neuron* **76**, 1057-1070.

[13] Lisman J, Buzsáki G, Eichenbaum H, Nadel L, Ranganath C, Redish AD (2017) Viewpoints: How the hippocampus contributes to memory, navigation and cognition. *Nat Neurosci* **20**, 1434-1447.

[14] Place R, Farovik A, Brockmann M, Eichenbaum H (2016) Bidirectional prefrontal-hippocampal interactions support context-guided memory. *Nat Neurosci* **19**, 992-994.

[15] Jin J, Maren S (2015) Prefrontal-hippocampal interactions in memory and emotion. *Front Syst Neurosci* **9**, 170.

[16] Eichenbaum H (2017) Prefrontal-hippocampal interactions in episodic memory. *Nat Rev Neurosci* **18**, 547-558.

[17] Simons JS, Spiers HJ (2003) Prefrontal and medial temporal lobe interactions in long-term memory. *Nat Rev Neurosci* **4**, 637-648.

[18] Soria Lopez JA, González HM, Léger GC (2019) Alzheimer's disease. *Handb Clin Neurol* **167**, 231-255.

[19] Baudic S, Barba GD, Thibaudet MC, Smagghe A, Remy P, Traykov L (2006) Executive function deficits in early Alzheimer's disease and their relations with episodic memory. *Arch Clin Neuropsychol* **21**, 15-21.

[20] Chao OY, de Souza Silva MA, Yang YM, Huston JP (2020) The medial prefrontal cortex - hippocampus circuit that integrates information of object, place and time to construct episodic memory in rodents: Behavioral, anatomical and neurochemical properties. *Neurosci Biobehav Rev* **113**, 373-407.

[21] Sánchez-Bellot C, AlSubaie R, Mishchanchuk K, Wee RWS, MacAskill AF (2022) Two opposing hippocampus to prefrontal cortex pathways for the control of approach and avoidance behaviour. *Nat Commun* **13**, 339.

[22] Gerlei KZ, Brown CM, Sürmeli G, Nolan MF (2021) Deep entorhinal cortex: From circuit organization to spatial cognition and memory. *Trends Neurosci* **44**, 876-887.

[23] Canto CB, Wouterlood FG, Witter MP (2008) What does the anatomical organization of the entorhinal cortex tell us? *Neural Plast* **2008**, 381243.

[24] Sekeres MJ, Winocur G, Moscovitch M (2018) The hippocampus and related neocortical structures in memory transformation. *Neurosci Lett* **680**, 39-53.

[25] Chao OY, Huston JP, Li JS, Wang AL, de Souza Silva MA (2016) The medial prefrontal cortex-lateral entorhinal cortex circuit is essential for episodic-like memory and associative object-recognition. *Hippocampus* **26**, 633-645.

[26] Basu J, Zaremba JD, Cheung SK, Hitti FL, Zemelman BV, Losonczy A, Siegelbaum SA (2016) Gating of hippocampal activity, plasticity, and memory by entorhinal cortex long-range inhibition. *Science* **351**, aaa5694.

[27] Brun VH, Leutgeb S, Wu HQ, Schwarcz R, Witter MP, Moser EI, Moser MB (2008) Impaired spatial representation in CA1 after lesion of direct input from entorhinal cortex. *Neuron* **57**, 290-302.

[28] Suh J, Rivest AJ, Nakashiba T, Tominaga T, Tonegawa S (2011) Entorhinal cortex layer III input to the hippocampus is crucial for temporal association memory. *Science* **334**, 1415-1420.

[29] Naber PA, Lopes da Silva FH, Witter MP (2001) Reciprocal connections between the entorhinal cortex and hippocampal fields CA1 and the subiculum are in register with the projections from CA1 to the subiculum. *Hippocampus* **11**, 99-104.

[30] Amaral DG, Dolorfo C, Alvarez-Royo P (1991) Organization of CA1 projections to the subiculum: A PHA-L analysis in the rat. *Hippocampus* **1**, 415-435.

[31] O'Mara S (2005) The subiculum: What it does, what it might do, and what neuroanatomy has yet to tell us. *J Anat* **207**, 271-282.

[32] Witter MP, Moser EI (2006) Spatial representation and the architecture of the entorhinal cortex. *Trends Neurosci* **29**, 671-678.

[33] de la Prida LM, Totterdell S, Gigg J, Miles R (2006) The subiculum comes of age. *Hippocampus* **16**, 916-923.

[34] Matsumoto N, Kitanishi T, Mizuseki K (2019) The subiculum: Unique hippocampal hub and more. *Neurosci Res* **143**, 1-12.

[35] O'Mara SM, Commins S, Anderson M, Gigg J (2001) The subiculum: A review of form, physiology and function. *Prog Neurobiol* **64**, 129-155.

[36] Aggleton JP, Christiansen K (2015) The subiculum: The heart of the extended hippocampal system. *Prog Brain Res* **219**, 65-82.

[37] Criscuolo C, Fontebasso V, Middei S, Stazi M, Ammassari-Teule M, Yan SS, Origlia N (2017) Entorhinal Cortex dysfunction can be rescued by inhibition of microglial RAGE in an Alzheimer's disease mouse model. *Sci Rep* **7**, 42370.

[38] Harris JA, Devidze N, Verret L, Ho K, Halabisky B, Thwin MT, Kim D, Hamto P, Lo I, Yu GQ, Palop JJ, Masliah E, Mucke L (2010) Transsynaptic progression of amyloid-β-induced neuronal dysfunction within the entorhinal-hippocampal network. *Neuron* **68**, 428-441.

[39] Olajide OJ, Suvanto ME, Chapman CA (2021) Molecular mechanisms of neurodegeneration in the entorhinal cortex that underlie its selective vulnerability during

the pathogenesis of Alzheimer's disease. *Biol Open* **10**, bio056796.

[40] Khan UA, Liu L, Provenzano FA, Berman DE, Profaci CP, Sloan R, Mayeux R, Duff KE, Small SA (2014) Molecular drivers and cortical spread of lateral entorhinal cortex dysfunction in preclinical Alzheimer's disease. *Nat Neurosci* **17**, 304-311.

[41] Yoshiyama Y, Higuchi M, Zhang B, Huang SM, Iwata N, Saido TC, Maeda J, Suhara T, Trojanowski JQ, Lee VM (2007) Synapse loss and microglial activation precede tangles in a P301S tauopathy mouse model. *Neuron* **53**, 337-351.

[42] Williams JB, Cao Q, Wang W, Lee YH, Qin L, Zhong P, Ren Y, Ma K, Yan Z (2023) Inhibition of histone methyltransferase Smyd3 rescues NMDAR and cognitive deficits in a tauopathy mouse model. *Nat Commun* **14**, 91.

[43] Zheng Y, Liu A, Wang ZJ, Cao Q, Wang W, Lin L, Ma K, Zhang F, Wei J, Matas E, Cheng J, Chen GJ, Wang X, Yan Z (2019) Inhibition of EHMT1/2 rescues synaptic and cognitive functions for Alzheimer's disease. *Brain* **142**, 787-807.

[44] Wang W, Cao Q, Tan T, Yang F, Williams JB, Yan Z (2021) Epigenetic treatment of behavioral and physiological deficits in a tauopathy mouse model. *Aging Cell* **20**, e13456.

[45] Qin L, Ma K, Wang ZJ, Hu Z, Matas E, Wei J, Yan Z (2018) Publisher Correction: Social deficits in Shank3-deficient mouse models of autism are rescued by histone deacetylase (HDAC) inhibition. *Nat Neurosci* **21**, 1139.

[46] Zhong P, Qin L, Yan Z (2020) Dopamine differentially regulates response dynamics of prefrontal cortical principal neurons and interneurons to optogenetic stimulation of inputs from ventral tegmental area. *Cereb Cortex* **30**, 4402-4409.

[47] Rapanelli M, Tan T, Wang W, Wang X, Wang ZJ, Zhong P, Frick L, Qin L, Ma K, Qu J, Yan Z (2021) Behavioral, circuitry, and molecular aberrations by region-specific deficiency of the high-risk autism gene Cul3. *Mol Psychiatry* **26**, 1491-1504.

[48] Tan T, Wang W, Liu T, Zhong P, Conrow-Graham M, Tian X, Yan Z (2021) Neural circuits and activity dynamics underlying sex-specific effects of chronic social isolation stress. *Cell Rep* **34**, 108874.

[49] Maffei A, Turrigiano GG (2008) Multiple modes of network homeostasis in visual cortical layer 2/3. *J Neurosci* **28**, 4377-4384.

[50] Zhong P, Yan Z (2016) Distinct physiological effects of dopamine D4 receptors on prefrontal cortical pyramidal neurons and fast-spiking interneurons. *Cereb Cortex* **26**, 180-191.

[51] Qin L, Ma K, Yan Z (2019) Chemogenetic activation of prefrontal cortex in shank3-deficient mice ameliorates social deficits, NMDAR hypofunction, and Sgk2 downregulation. *iScience* **17**, 24-35.

[52] Qin L, Williams JB, Tan T, Liu T, Cao Q, Ma K, Yan Z (2021) Deficiency of autism risk factor ASH1L in prefrontal cortex induces epigenetic aberrations and seizures. *Nat Commun* **12**, 6589.

[53] Wang W, Rein B, Zhang F, Tan T, Zhong P, Qin L, Yan Z (2018) Chemogenetic activation of prefrontal cortex rescues synaptic and behavioral deficits in a mouse model of 16p11.2 deletion syndrome. *J Neurosci* **38**, 5939-5948.

[54] Wang ZJ, Shwani T, Liu J, Zhong P, Yang F, Schatz K, Zhang F, Pralle A, Yan Z (2022) Molecular and cellular mechanisms for differential effects of chronic social isolation stress in males and females. *Mol Psychiatry* **27**, 3056-3068.

[55] Wei J, Zhong P, Qin L, Tan T, Yan Z (2018) Chemicogenetic restoration of the prefrontal cortex to amygdala pathway ameliorates stress-induced deficits. *Cereb Cortex* **28**, 1980-1990.

[56] Masurkar AV, Srinivas KV, Brann DH, Warren R, Lowes DC, Siegelbaum SA (2017) Medial and lateral entorhinal cortex differentially excite deep versus superficial CA1 pyramidal neurons. *Cell Rep* **18**, 148-160.

[57] Valero M, de la Prida LM (2018) The hippocampus in depth: A sublayer-specific perspective of entorhinal-hippocampal function. *Curr Opin Neurobiol* **52**, 107-114.

[58] Stafstrom CE (2005) The role of the subiculum in epilepsy and epileptogenesis. *Epilepsy Curr* **5**, 121-129.

[59] Oakley H, Cole SL, Logan S, Maus E, Shao P, Craft J, Guillozet-Bongaarts A, Ohno M, Disterhoft J, Van Eldik L, Berry R, Vassar R (2006) Intraneuronal beta-amyloid aggregates, neurodegeneration, and neuron loss in transgenic mice with five familial Alzheimer's disease mutations: Potential factors in amyloid plaque formation. *J Neurosci* **26**, 10129-10140.

[60] Robinson JC, Brandon MP (2021) Skipping ahead: A circuit for representing the past, present, and future. *Elife* **10**, e68795.